Modeling of Dislocation Loop Growth and Transient Enhanced Diffusion in Silicon for Amorphizing Implants

Alp H. Gencer and Scott T. Dunham
Department of Electrical and Computer Engineering
Boston University, Boston, MA 02215

It has been observed that dislocation loops form and grow during annealing of silicon wafers implanted at doses above the amorphization threshold. Dislocation loops can act to store interstitials for prolonged periods of anneals, sustaining an interstitial super-saturation and thus causing substantial transient enhanced diffusion (TED). We have developed a comprehensive model which, in combination with a model and parameters for {311} defects from previous work, accounts for the formation and evolution of dislocation loops during ion implant annealing, as well as giving the correct TED behavior.

1. INTRODUCTION

It is well known that ion implantation at high doses produces an amorphous layer of silicon extending from the surface down to a depth that depends on the implant dose and conditions. During subsequent annealing of amorphized samples the amorphous region recrystallizes rapidly to form a defect free region. However, the damage of the implant that extends beyond the amorphous layer remains, and excess interstitials in this region, also called the end of range (EOR) region, agglomerate to form stable clusters, namely dislocation loops.[1] As annealing proceeds, they undergo Ostwald ripening and become extremely stable, withstanding even high thermal budget anneals. Dislocation loops have a significant impact on device characteristics both directly as recombination centers as well as through their interactions with point defects and thus dopant diffusion, so accurate modeling of their evolution is important.

Experimental observations have revealed that during annealing of samples implanted at doses below the amorphization threshold {311} defects form.[2] For doses around the amorphization threshold, both dislocation loops and {311} defects have been observed to co-exist in the wafer.[3] It has also been reported that {311} defects can transform into dislocation loops by a reaction called unfaulting,[4] suggesting a strong link between {311} defects and dislocation loops. Thus, a model for dislocation loop nucleation and growth should definitely include {311} defect kinetics as well. It is a challenge to predict the conditions under which dislocation loops, {311} defects or a mixture of the two will form.

2. MODEL

Our approach was to extend our model for {311} defects[5] to include dislocation loops as well. We did this by assuming that all defects that are smaller than a certain size (n_c) are {311} defects, and those above it are dislocation loops. This assumption is probably an oversimplification of the real kinetics, since it assumes instantaneous transfer from {311} defects into loops once n_c is crossed; yet it allows us to have a single extended defect distribution and keep our simulations simple.

2.1. Energetics of the model

Our model treats this extended defect population by explicitly considering precipitates of different sizes as independent species (f_n) and accounts for their kinetics by considering the attachment and emission of interstitial atoms.

The driving force for extended defect formation is the minimization of the free energy of the system, where the free energy of a size n extended defect is given by:

$$\Delta G_n = -nkT \ln \frac{C_{\mathrm{I}}}{C_{\mathrm{ss}}} + \Delta G_n^{\mathrm{exc}} \tag{1}$$

Here, C_{ss} is the "solid solubility" of interstitials associated with the formation of extended defects and $\Delta G_n^{\mathrm{exc}}$ is the excess surface and strain energy of a size n extended defect. Since our distribution is a mix of {311} defects and dislocation loops, the excess energy will be the minimum of the energies associated with each defect. Thus for $n < n_c$ the {311} defect energy will be smaller, so that it is more favorable to stay as a {311} defect; and for $n > n_c$, the loop energy will be smaller, so that it is more favorable to transform into a loop. We assumed $\Delta G_n^{\mathrm{exc}}$ to have a polynomial form:

$$\Delta G_n^{\mathrm{exc}} = \begin{cases} a_0 n^{\beta_0} + a_1 n^{\beta_1} + a_2 n^{\beta_2} + a_3 n & \text{for } n < n_c \\ b_0 n^{\beta_0} + b_1 & \text{for } n \geq n_c \end{cases} \tag{2}$$

It can be argued that $\beta_0 = 0.5$ since dislocation loops are disc-like defects and the excess surface energy will essentially be proportional to the perimeter of the disc as the defect size increases. We have chosen $\beta_1, \beta_2 < 0$ as corrections for the small size behavior. It may be readily observed that the linear term in $\Delta G_n^{\mathrm{exc}}$ can be incorporated into C_{ss}, but still a_3 is necessary to bridge the gap between C_{ss} for {311} defects and dislocation loops and to use a single C_{ss} for the whole distribution. The coefficients a_0, a_1, a_2, a_3 and b_0, b_1 are related by the fact that the energy and its derivative have to be continuous at $n = n_c$.

2.2. Kinetics of the model

The main reaction in the system is the attachment and emission of interstitials to and from the extended defects. If I_n denotes the net growth rate from size n to $n+1$, we may write the following equation:

$$I_n = D_{\mathrm{I}} \lambda_n \left(C_{\mathrm{I}} f_n - C_n^* f_{n+1} \right) \tag{3}$$

The kinetic growth factor, λ_n, incorporates effects of both diffusion to the precipitate/silicon interface and the reaction at the interface. λ_n is calculated based on solving the steady-state diffusion equation in the neighborhood of a disc-like planar defect.[6] C_n^* represents the interstitial concentration at which a size n defect would gain no energy by growing from size n to size $n+1$:

$$C_n^* = C_{\mathrm{ss}} \exp \left(\frac{\Delta G_{n+1}^{\mathrm{exc}} - \Delta G_n^{\mathrm{exc}}}{kT} \right) \tag{4}$$

To integrate the our model into a diffusion equation solver, we follow the moment-based approach[7] and keep track of only the lowest three *moments* of the distribution ($m_i = \sum_{n=2}^{\infty} n^i f_n$, where $i = 0, 1, 2$) with an appropriate closure assumption. In particular, the closure assumption used is that the distribution is the one that minimizes the free energy, given the moments. The resulting system has the following set of continuity equations:

$$\begin{aligned}
\frac{\partial m_0}{\partial t} &= I_1 \\
\frac{\partial m_1}{\partial t} &= 2I_1 + \sum_{n=2}^{\infty} I_n \\
\frac{\partial m_2}{\partial t} &= 4I_1 + \sum_{n=2}^{\infty} I_n(2n+1) \\
\frac{\partial C_{\mathrm{I}}}{\partial t} &= D_{\mathrm{I}}\nabla^2 C_{\mathrm{I}} - 2I_1 - \sum_{n=2}^{\infty} I_n
\end{aligned} \tag{5}$$

Note that with the closure assumption, the sums over the I_n can be calculated from the three moments,[7] but require the solution of a non-linear equation system at every time step and each grid point. To make the simulation computationally efficient, the sums are pre-tabulated for a range of m_i values and interpolation from these values is used during the simulation.[8]

3. PARAMETERS AND INITIAL CONDITIONS

As in our previous work,[5] we use the film segregation model as boundary conditions at the surface.[9] For bulk point defect parameters (diffusivities and equilibrium concentrations of interstitials and vacancies), we use the values calculated from metal diffusion (Zn, Au and Pt).[10,11] We furthermore assume that both I/V recombination and interstitial precipitation are diffusion limited.

The initial point defect profiles were obtained from Monte-Carlo simulations using TRIM-CSR and UT-MARLOWE. During annealing of amorphizing doses, the amorphous regrows during temperature ramp-up, leaving no excess point defects in this region. Thus, all net excess interstitials will be in the EOR region. The amorphous/crystalline interface is usually assumed to be at the point where the total vacancy concentration due to implant damage falls below a certain fraction of atomic density of silicon ($5 \times 10^{22}\,\mathrm{cm}^{-3}$). Reported values for this fraction are around 10%, which results in a net excess interstitial dose of $1.4 \times 10^{14}\,\mathrm{cm}^{-2}$ for an implant of $1 \times 10^{16}\,\mathrm{cm}^{-2}$ Si at 50 keV (Fig. 1).

However, dislocation loop data by Pan *et al.*[1] suggest that under these conditions there are approximately $7.3 \times 10^{14}\,\mathrm{cm}^{-2}$ interstitials in dislocation loops. Thus, even if we assume that all excess interstitials would precipitate into dislocation loops, a 10% threshold would still predict a too low dose. We found it necessary to increase the threshold to 60% to obtain the correct dose. This discrepancy may be justified by assuming that some healing takes place during the implantation process itself, resulting in a lower damage level than that calculated by the Monte-Carlo implant simulations.

4. RESULTS

Pan *et al.*[1] implanted $1 \times 10^{16}\,\mathrm{cm}^{-2}$ Si into silicon at 50 keV and annealed the samples at 750°C. They measured the resulting dislocation loop distributions using TEM. We took the form of the {311} defect energy from previous work,[5] and chose the crossover from {311} defects to dislocation loops to occur at $n = 3000$, which corresponds to a maximum {311}

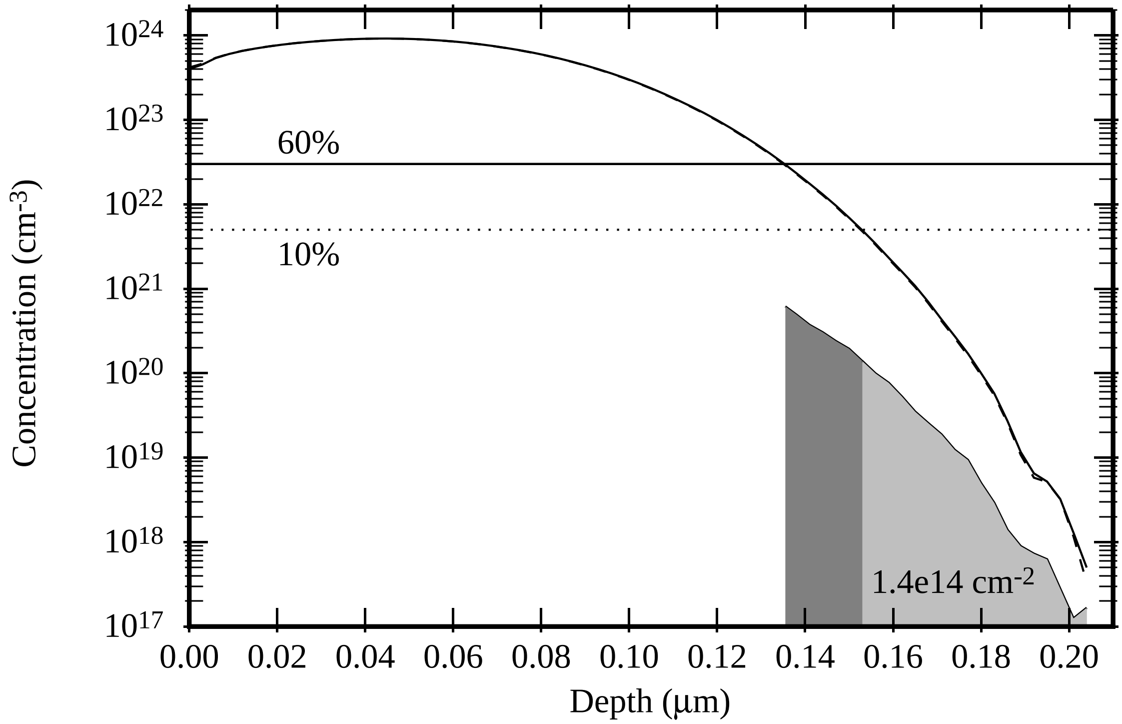

Fig. 1: TRIMCSR simulation of point defect concentrations resulting from a $1 \times 10^{16}\,\mathrm{cm}^{-2}$ Si implant at 50 keV. The total interstitial and vacancy concentrations before regrowth are nearly equal. The point defect concentrations exceed the silicon atom density in the peak region because multiple displacements are counted separately. The horizontal lines represent 10% and 60% thresholds for amorphization and the shaded regions show the corresponding net interstitial excess after regrowth.

defect length of 120 nm. It can be argued that C_{ss} for loops should be just C_{I}^{*}, since an infinite size perfect loop is nothing but an extra plane in silicon. For partial loops C_{ss} should be slightly higher, but small changes in C_{ss} had no significant effect in our simulation results.

Our results show that we were able to correctly model the approximately constant number of interstitials in dislocation loops (Fig. 2), as well as the Ostwald ripening behavior (Fig. 3). The extremely slow dissolution rate of dislocation loops stems from the facts that they can grow very large and C_{ss} for loops is equal to C_{I}^{*}. This results in C_{n}^{*} for loops being very close to C_{I}^{*}, so that they sustain a very small super-saturation of interstitials. Since these loops are deep in the substrate and sustain only a minimal super-saturation, the flux to the surface is small and thus they dissolve extremely slowly.

We applied the same model to TED data for amorphizing doses. We used data from Huang,[12] who reported the total profile movement of a deep boron marker layer during annealing at 750°C, following an implant of $1 \times 10^{16}\,\mathrm{cm}^{-2}$ Si at 50 keV. It can be observed that the model does an excellent job in predicting the amount of profile movement under these conditions (Fig. 4). The model gives the right magnitude for the observed enhancements, as well as the length of time TED lasts.

5. SUMMARY

In summary, we were able to model the formation and evolution of dislocation loops by extending our model for {311} defects to a distribution which is a mixture of the two kinds of extended defects. We were able to model the observed Ostwald ripening behavior, and apply

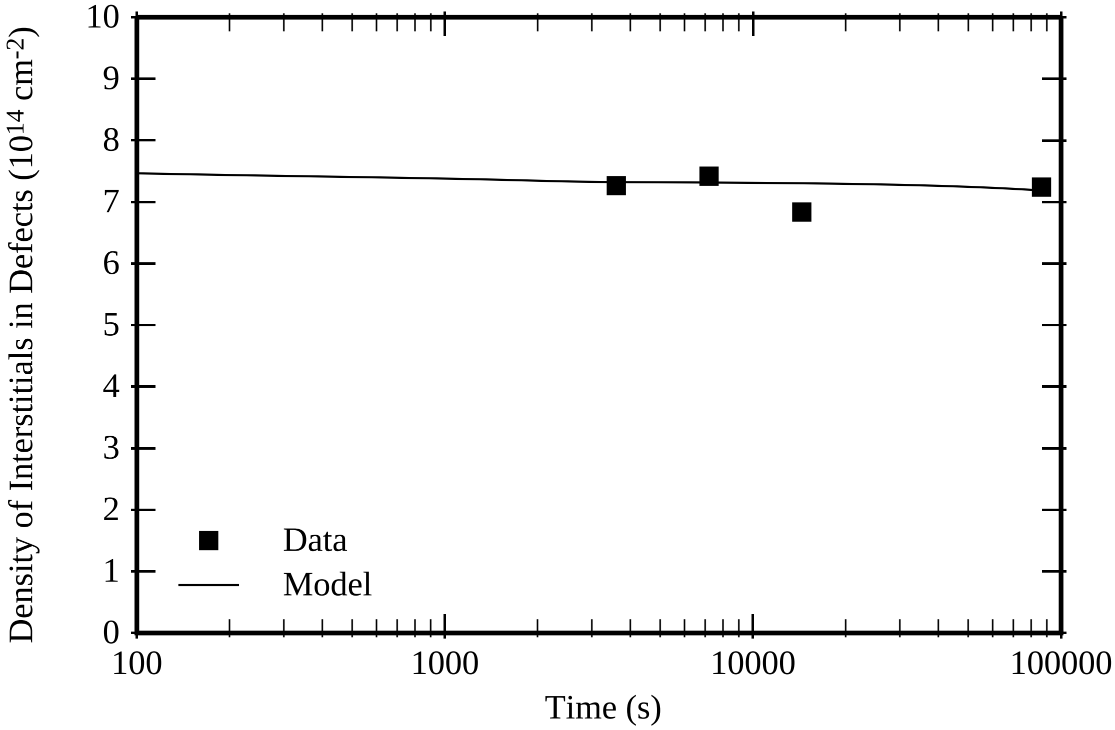

Fig. 2: Evolution of density of interstitials in extended defects (m_1) and comparison to model. Data from Pan *et al.*[1] for $1 \times 10^{16}\,\mathrm{cm}^{-2}$ Si implant at $50\,\mathrm{keV}$ with annealing at $750°\mathrm{C}$.

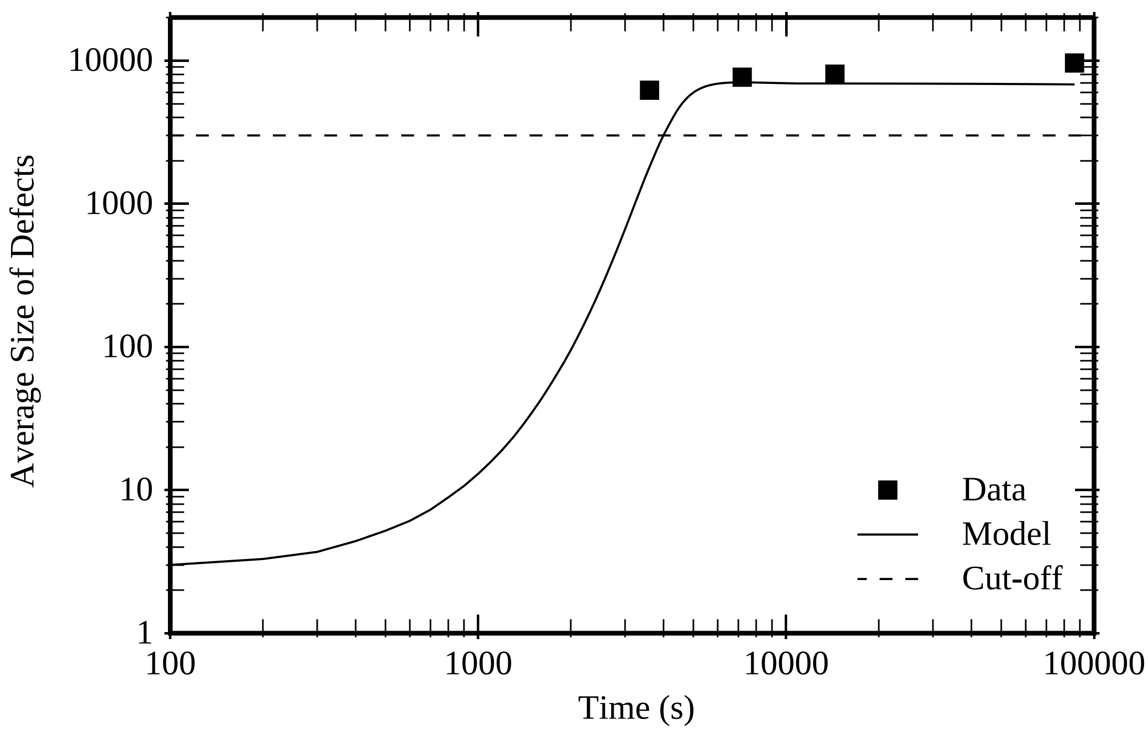

Fig. 3: Evolution of average defect size (m_1/m_0) for $1 \times 10^{16}\,\mathrm{cm}^{-2}$ Si implants at $50\,\mathrm{keV}$ and comparison to data from Pan *et al.*[1] The dashed line represents the division between distributions dominated by {311} defects and dislocation loops.

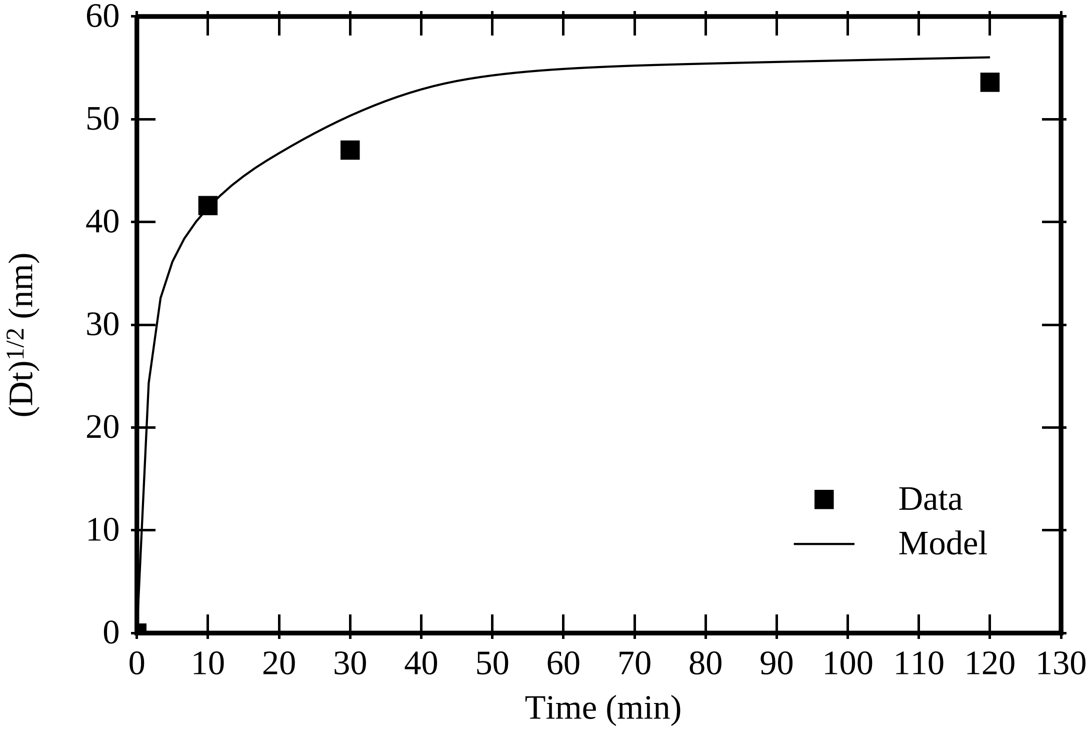

Fig. 4: Total broadening of a deep B marker profile due to implantation of $1 \times 10^{16}\,\mathrm{cm}^{-2}$ Si at 50 keV with annealing at 750°C. Data from Huang[12] and comparison to model prediction.

the model to TED data with excellent results. The model assumes that there is a strong link between {311} defects and dislocation loops and is able to account for the kinetics of both types of defects under the same framework.

This work was supported by the Semiconductor Research Corporation.

[1] G.Z. Pan, K.N. Tu, and S. Prussin, *Appl. Phys. Lett.* **68**, 1654 (1996).

[2] D.J. Eaglesham, P.A. Stolk, H.J. Gossmann, and J.M. Poate, *Appl. Phys. Lett.* **65**, 2305 (1994).

[3] K.S. Jones, J. Lui, L. Zhang, V. Krishnamoorthy, and R.T. DeHoff, *Nuc. Inst. and Meth. B* **106**, 227 (1995).

[4] D.J. Eaglesham, P.A. Stolk, H.J. Gossmann, T.E. Haynes, and J.M. Poate, *Nuc. Inst. and Meth. B* **106**, 191 (1995).

[5] A.H. Gencer and S.T. Dunham, *J. Appl. Phys.* (1997). To appear in the January 1st, 1997 issue.

[6] S.T. Dunham, *Appl. Phys. Lett.* **63**, 464 (1993).

[7] I. Clejan and S.T. Dunham, *J. Appl. Phys.* **78**, 7327 (1995).

[8] A.H. Gencer. *DOPDEES User's Manual* (1996).

[9] A.M. Agarwal and S.T. Dunham, *J. Appl. Phys.* **78**, 5313 (1995).

[10] H. Bracht, N.A. Stolwijk, and H. Mehrer, *Phys. Rev. B* **52**, 16542 (1995).

[11] H. Zimmermann and H. Ryssel, *Applied Physics A* **55**, 121 (1992).

[12] R.A. Huang, Ph.D. thesis, Stanford University (1994).